Hindawi
Journal of Energy
Volume 2020, Article ID 8844433, 11 pages
https://doi.org/10.1155/2020/8844433

Research Article

Numerical Analysis of Heat Exchanger for Spray-Assisted Low-Temperature Desalination System

Amour Othman Muhunzi,[1,2] **Yusufu Abeid Chande Jande**,[1] **and Revocatus Lazaro Machunda**[3]

[1]*Department of Materials and Energy Sciences and Engineering, The Nelson Mandela African Institution of Science and Technology, P.O. Box 447, Arusha, Tanzania*
[2]*Department of Technical Services, The Government Agency for Tractors and Farm Machineries Services, P.O. Box 1064, Zanzibar, Tanzania*
[3]*Department of Environmental Sciences and Engineering, The Nelson Mandela African Institution of Science and Technology, P.O. Box 447, Arusha, Tanzania*

Correspondence should be addressed to Amour Othman Muhunzi; muhunzia@nm-aist.ac.tz

Received 18 April 2020; Revised 19 August 2020; Accepted 24 September 2020; Published 16 November 2020

Academic Editor: Ciro Aprea

A numerical study for heat exchanger for spray-assisted low-temperature desalination system is presented for an existing low-temperature desalination unit at Arusha Technical College. This is aimed at recognizing the effect of mass flow and physical parameters like tube layout (diameter and length) on the overall heat transferred and the pressure drop in the shell-and-tube heat exchanger (STHX), as well as the impact of these parameters on the heat transfer coefficient and the overdesign of the STHX. Also, the study provides a suitable mathematical model for the replacement of the current condensation unit which tends to reduce energy consumption by reducing some of the electrical components in the system. A Math CAD model was developed using the Delaware method to obtain the mentioned parameters. The results show that at 0.8 kg/s flow rate a maximum heat transfer coefficient of 23212 W/m^2K is achieved in a minimum diameter of 10 mm within a maximum tube length of 1000 mm heat exchanger and the pressure drop seems to be very low in a range of 0.328-0.957 Pa from all configurations. The configuration with 1000 mm tube length and 10 mm diameter performed well on the mass flow of 0.3 kg/s-0.8 kg/s by providing a suitable overall heat transfer coefficient of 2306-2539 W/m^2K, while 12.8 is a maximum overdesign coefficient achieved on 0.8 kg/s mass flow. The study results show the possibility of using STHX instead of the current condensation unit in implementing a proposed system layout with the minimum effect of energy consumption.

1. Introduction

The present society demands the efficient utilization of energy and at the same time reducing environmental impact to contribute to sustainable economic development. The increase of freshwater demand is mainly caused by the development of world industries and human population growth, while potable water is one of the key resources for the existence of human beings [1]. Desalination of brackish or seawater is an important approach to solve the water resource dearth. We may categorize the desalination process as thermal and nonthermal based on energy consumption [2].

Spray-assisted low-temperature phase-change desalination technique is the thermal-based method that makes no boundary upon heat and mass transfer mechanism and eliminates the contribution of mechanical energy input [3]. This technology comprises two main units to reach the freshwater, namely, evaporation unit and condensation unit [4]. Fortunately, solar energy can either be used directly or indirectly in supplying thermal energy to an evaporation unit as used in vaporization of liquid

into vapor and cause steam formation [5]. However, the heat exchange process occurs in the condensation unit by exchanging steam temperature with that of cooling media (gas or liquid) and condensing the steam into liquid freshwater [6].

Literature shows some of the experimental and numerical studies done by some researchers concerned with the condensation unit in different desalination systems. Alsadaie and Mujtaba [7] through the multistage flash (MSF) desalination developed a dynamic fouling model of the heat exchanger, reaction and diffusion mechanisms were included to investigate the effect of surface temperature and flow velocity, and the fouling results made a clear agreement with the literature on current studies. The cryogenic refrigeration unit embedded with multieffect desalination unit hybrid system was designed by Ghorbani et al. [8] which analyzed the thermos-economic.

In adsorption desalination, Elsayed et al. [9] used an aluminum fumarate metal-organic framework in experimental observation of cooling water desorption, adsorption, and condensation. Olkis et al. [10] analyzed the performance of an adsorption heat transformer through the usage of benchmarking material silica gel in the production of freshwater together with the cooling process as done by Thu et al. [11] and achieved a performance ratio of 0.60 at the inlet temperature of 80°C. Also, silica gel was proposed by Rezk et al. [12] to be employed in solar-assisted adsorption desalination cooling for the performance maximization; the results show an improvement of 70% increase in specific cooling power, 0.961 coefficient of performance, and 6.9 m^3/day/ton specific daily water production.

Another study was done by Woo et al. [13] on a silica gel-based adsorption cooling cum desalination system concerned with the performance effect, operating pressure, and brine concentration. Towards eco-friendliness, David et al. [14] recovered the waste heat through the method of evaporative condenser cum thermal desalination. An experimental study was conducted by Rabhi et al. [15] on the external condenser and pin fin absorber from a modified solar still; the evaluation was based on the performance of water production and the thermal behavior.

Chandrakanth et al. [16] computed the tube-side pressure drop and heat transfer area respective in the optimization of the shell and tube condenser process parameters and geometric used in thermal desalination plants. The optimum pressure drop vs. heat transfer area was concluded from the second law analysis to overcome the trade-off in between. Via stoichiometric process in the spray flash desalination system, a water level model for after condenser was constructed by Matsuda et al. [17]; the results show the proper model that could improve the system behavior.

From the above literature, the flash evaporator has been reported from many theoretical and experimental studies as an essential unit in the low-temperature desalination technology. But there is no specific study that discusses the condensation unit on flash evaporation desalination technology. Moreover, currently, there is an existing low-temperature desalination unit at Arusha Technical College (ATC), which uses more energy at the condensation unit. Thus, this paper focuses on a heat exchanger design for spray-assisted low-temperature desalination, whereby the pressure drop, heat transfer coefficient, overall heat transfer coefficient, oversurface, and overdesign are the main concern. The heat exchanger is designed to reduce the level of energy consumption, allowing for a smooth working environment of the desalination unit.

2. Modification of Existing System Configuration

Figure 1 shows a schematic of the current layout with several electric components, namely, blower, feed pump, filter with a suction fan, cooling water circulation pump, and condenser with a suction fan. These components make a high level of energy intensity. Here, saline water from the source chamber is pumped into the flash chamber via nozzles. The sprayed flash occurs and the small droplets absorb the thermal energy in the flash chamber to form steam. Steam is escaping the chamber by passing between the chamber's walls, sucked through filter suction fan directly to the filter, then sucked by condenser suction fan and condensed, and finally stored as freshwater in a distillate reservoir. The steam is condensed when the cold water is circulated in the condenser from the water circulator tank via a second feed pump. At the same time, the condenser suction fan sucks the steam from the filter to speed up the process in which much steam is allowed to escape into the atmosphere. Both condenser and filter suction fans increase the amount of energy consumption on the system.

Figure 2 shows a schematic of a proposed layout that remains with the blower and the feed pump only which may alleviate the energy consumption through the implementation of the heat exchanger as a condensation unit. Now, source water from the source chamber is pumped to evacuated tube collector through the heat exchanger then fed to a flash chamber via nozzles. As usual, the sprayed flash occurs and absorbs the thermal energy in the flash chamber to form steam. Steam escapes the chamber by passing at the top, condensed by exchanging heat with cold water from the source at the heat exchanger, and stored as a freshwater. The blower is embedded with a flash chamber to increase temperature and relative humidity [18]. The heat exchanger acts as a condenser and at the same time becomes a preheater for the incoming cold water. The evacuated tube collector (also a preheater) raises further the temperature of the feed water before it is fed into the flash chamber.

3. Heat Exchanger

The heat exchange process takes place between two or more channels at different temperatures when fluids of the channels exchange their temperature by passing through a heat exchanger [19]. The heat exchanger is a piece of equipment that permits heat transfer and often goes together with mass transfer [20]. The equipment has been used in various industries including processing industries, power plants, and many other industries [21]. Among the several heat exchanger

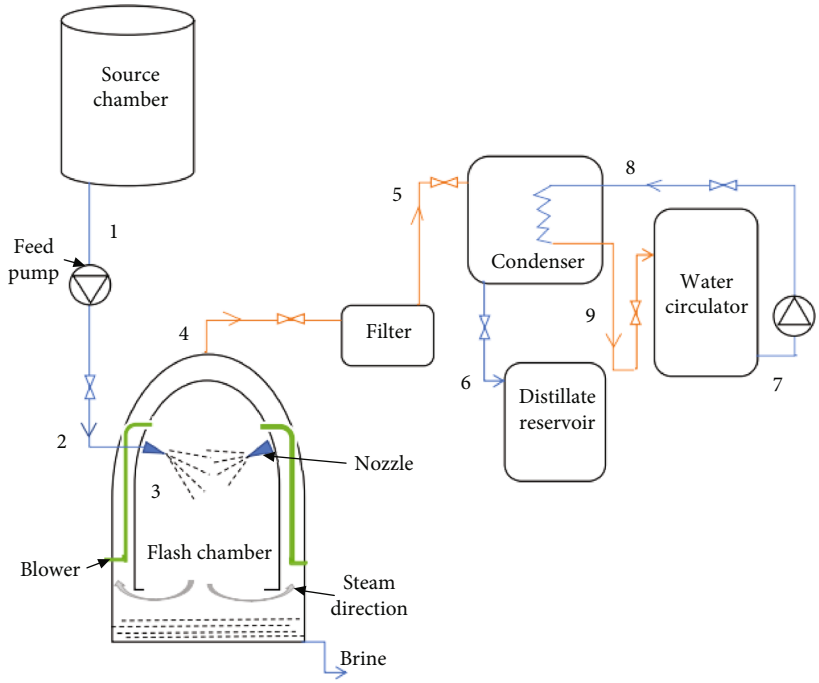

Figure 1: The current layout of spray flash evaporation system.

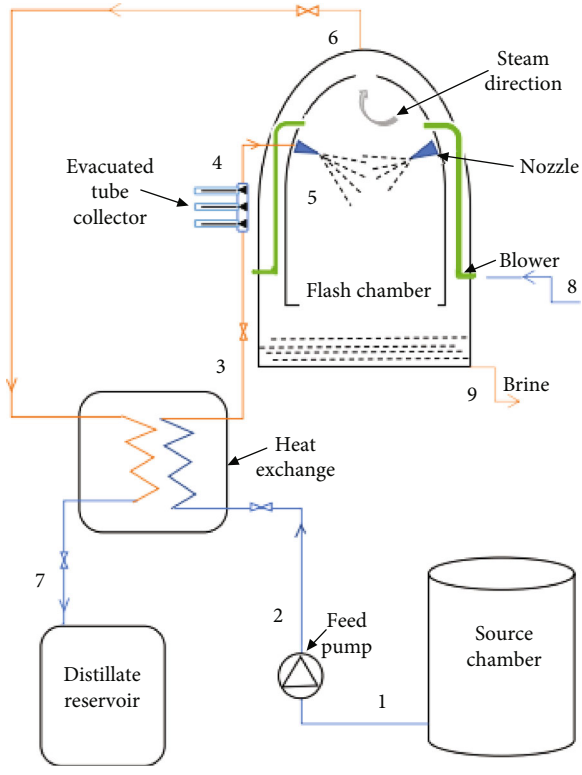

Figure 2: Proposed layout of spray flash evaporation system.

models, shell-and-tube heat exchangers (STHX) are the best [22] and widely used [23]. Also, it can be constructed easily in an extensive range of sizes compared to other categories [24]. A model of the shell-and-tube heat exchanger is shown in Figure 3(b).

4. Methodology

Thermal conductivity, density, viscosity, and specific heat capacity of the cold and hot fluid stream were among the factors estimated in the primary stage in the STHX design as can be seen in Table 1, taken from the existing evaporator which appeared in Figure 3(a). Double shell passes were taken into account, and a triangular pitch of 1.25 space between tube to tube centers was considered for the analysis. A single segmental baffle was chosen for ease of maintenance and high thermal features. U-tube (tube sheet) was used to permit a distinction of thermal expansion. Moreover, the outlet temperatures 29 and 28°C (t_7 and t_3) for steam and water, respectively, were assumed to control the output and easy computation as shown in Figure 3(b).

4.1. Thermal Design. The temperature difference on the tube side or that of shell side was used to define the sensible heat transfer rate of a heat exchanger. The cold and hot fluid stream loads were calculated using equation (1) as described by [25]

$$Q = \dot{m}_f Cp_f (t_3 - t_2) = \dot{m}_g Cp_g (t_6 - t_7), \quad (1)$$

where $\dot{m}_g$ and $\dot{m}_f$ are mass flow rate of steam and water, respectively, Q is heat transfer rate, Cp_g and Cp_f are specific heat capacity of steam and water, respectively, t_3 and t_2 are outlet and inlet temperature of the water, and t_7 and t_6 are outlet and inlet temperature of steam, respectively.

Equation (2) is used to calculate the logarithmic mean temperature difference (ΔT_{lm}) to use in estimating the true temperature difference in equation (3) by applying a correction factor (F_t) in the design of shell and tube

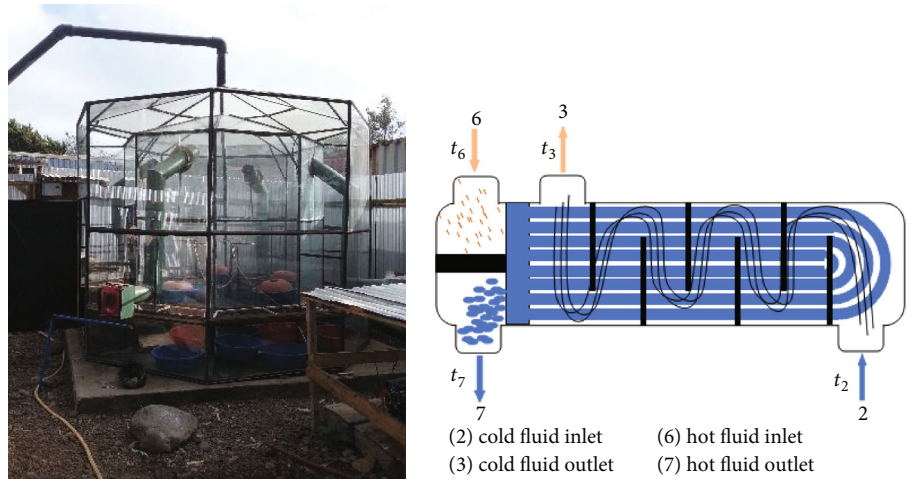

Figure 3: (a) Low-temperature evaporator in Arusha Technical College, Tanzania. (b) Shell-and-tube heat exchanger model.

Table 1: Physical parameters of steam and water were taken from the steam evaporator.

System components	$\dot{m}$ (kg/s)	T_{inlet} (°C)	T_{outlet} (°C)	ρ (kg/m^3)	Cp (kJ/kg K)	μ (Pa s)	k (W/m K)	$R_{fouling}$ (m^{2}K/W)
Steam	0.024	60	29	0.191	1914	0.000011	0.023	0.00009
Water	0.1-0.8	25	28	996.4	4179	0.00089	0.597	0.00018

exchangers to allow for the departure from the true counter-current flow:

$$\Delta T_{lm} = \frac{(t_6 - t_3) - (t_7 - t_2)}{\ln\left((t_6 - t_3)/(t_7 - t_2)\right)}, \quad (2)$$

$$\Delta T_m = F_t \Delta T_{lm}. \quad (3)$$

4.2. Overall Heat Transfer Coefficient Assessment. To attain a preliminary appraisal for the size of the STHX, an approximate value for the overall heat transfer coefficient (U_o) is used. According to the working fluid, the range is 1500-4000 W/m^{2}K as stated by [26]

$$A = \frac{Q}{U_o \Delta T_m}, \quad (4)$$

where A is the heat transfer area, Q is the heat transfer rate, U_o is the pilot overall heat transfer coefficient, and ΔT_m is the true temperature difference.

4.3. Tube-Side Calculations. From the standard tube layouts, the empirical equation (6) was used to determine bundle diameter. n_1 and K_1 in the equation are coefficients determined by the tube layout and the number of tube passes from Table 2 for triangular pitch and square pitch, while the number of tubes (n_t) was calculated by dividing the total heat transfer area (A) and the tube outer surface area (A_t) as shown in

Table 2: Coefficients n_1 and K_1 for use in equation (10) [27].

Tube passes	1	2	4	6	8
Square pitch					
n_1	2.207	2.291	2.263	2.617	2.643
K_1	0.215	0.156	0.158	0.0402	0.0331
Triangular pitch					
n_1	2.142	2.207	2.285	2.499	2.675
K_1	0.319	0.249	0.175	0.0743	0.0365

$$n_t = \frac{A}{A_t}, \quad (5)$$

$$D_b = d_o \left(\frac{n_t}{K_1}\right)^{1/n_1}. \quad (6)$$

The heat transfer coefficient (h_t) of the hot fluid stream was determined by using equation (7) [28]. It is a function of a tube inner diameter (d_i), tube side Prandtl number (Pr_t), and tube side Reynolds number (Re_t). Also, nondimensional numbers like hot fluid thermal conductivity (k_g), hot

fluid viscosity (μ_g), and water viscosity (μ_w) are included in the equation [29].

$$h_t = \frac{k_g}{d_i} \mathrm{Re}_t^{0.8} \mathrm{Pr}_t^{0.33} \left(\frac{\mu_g}{\mu_w}\right)^{0.14}. \quad (7)$$

4.4. Shell-Side Equations. The shell diameter is calculated as follows:

$$D_s = D_c + D_b, \quad (8)$$

$$D_c = c_1 + m_1 D_b. \quad (9)$$

In the above equations, D_s is a shell diameter and D_c is a clearance between the diameter of the shell and a tube bundle diameter D_b, where the values of c_1 and m_1 are presented in Table 3. c_1 and m_1 are empirical coefficients that relate to the head type designed in the STHX.

The heat transfer coefficient (h_s) on the shell side was determined from equation (10), where k_f is a cold fluid thermal conductivity, d_e is a shell equivalent diameter, J_h is a Colburn factor, Pr_s is a shell side Prandtl number, and μ_f and μ_w are cold fluid and water viscosity, respectively.

$$h_s = \frac{k_f}{d_e} J_h \mathrm{Pr}_s^{0.33} \left(\frac{\mu_f}{\mu_w}\right)^{0.14}. \quad (10)$$

4.5. Overall Coefficient Calculations. In this, the required overall heat transfer coefficient U_{req} was calculated using

$$U_{req} = \frac{Q}{\pi n_t d_o l_t \Delta T_m}. \quad (11)$$

The clean overall heat transfer coefficient U_c was calculated using

$$U_c = \left(\frac{d_o}{h_t d_i} + \frac{d_o \ln(d_o/d_i)}{2k} + \frac{1}{h_s}\right)^{-1}. \quad (12)$$

If $U_{req} < U_c$, the following step was considered.

Then, the design overall heat transfer coefficient was determined through

$$U_d = \left(\frac{d_o}{h_t d_i} + \frac{d_o \ln(d_o/d_i)}{2k} + \frac{1}{h_s} + \frac{R_v d_o}{d_i} + R_f\right)^{-1}. \quad (13)$$

If $U_d \geq U_{req}$, the next step was worthy to be carried out.

Overdesign is computed in equation (14). The final design safety margin is provided by overdesign in which the required fouling compensation is represented. Oversurface deals with exchanger surface area and depends on the wall and film resistances and fouling allowance; it can be obtained through equation (15).

$$O_{des} = \frac{U_d}{U_{req}} - 1, \quad (14)$$

Table 3: Coefficients c_1 and m_1 for use in equation (9) [30].

Head type	c_1	m_1
Outside packed head	0.038	0.0
Pull through floating head	0.0862	0.009
Split ring floating head	0.0446	0.027
U-tube or fixed head	0.008	0.01

$$O_{sur} = \frac{U_c}{U_{req}} - 1. \quad (15)$$

4.6. Pressure Drop Calculations

4.6.1. Tube-Side Pressure Drop. A pressure drop (ΔP_i) of the hot fluid stream was computed as shown in equation (16), where f_t is a Darcy friction factor, s_t is the specific gravity in the tube side, l_t is the tube length, G_g is the hot fluid mass velocity, n_p is the number of tube passes, and d_i is the tube internal diameter.

$$\Delta P_i = \frac{f_t l_t G_g^2 n_p}{7.5 \times 10^{12} d_i s_t}. \quad (16)$$

The tube entrance, exit, and return losses can be computed through

$$\Delta P_r = 1.334 \times 10^{-13} (2n_p - 1.5) \frac{G_g}{s_t}. \quad (17)$$

The pressure loss (ΔP_{nt}) in the tube side nozzles is considered through equation (18), where G_{nt} is a tube side nozzle mass velocity and n_s is the number of tube passes.

$$\Delta P_{nt} = 2.0 \times 10^{-13} \frac{n_s G_{nt}^2}{s_t}. \quad (18)$$

Equation (19) was used to evaluate the total pressure drop (ΔP_t) across the hot fluid stream on the tube side as presented below:

$$\Delta P_t = \Delta P_i + \Delta P_r + \Delta P_{nt}. \quad (19)$$

4.6.2. Shell-Side Pressure Drop. Equation (20) was used to find the initial shell side pressure losses (ΔP_o), where s_s is a specific gravity in the shell side, f_s is the friction factor, d_e is the equivalent diameter, n_b is the number of the baffle, and D_s is a shell diameter.

$$\Delta P_o = \frac{f_s (G_g)^2 D_s (n_b + 1)}{7.5 \times 10^{12} d_e s_s}. \quad (20)$$

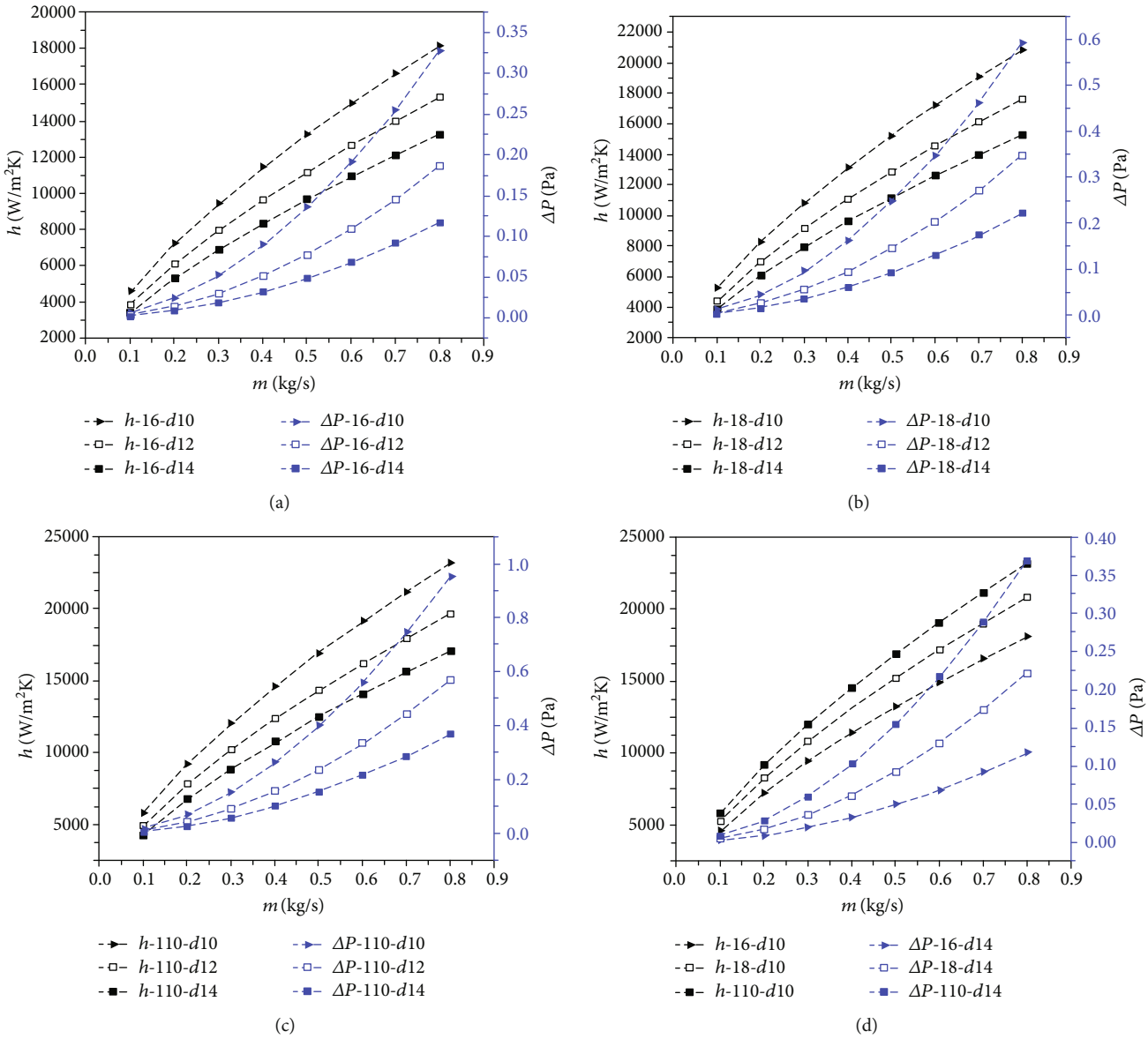

Figure 4: Pressure drop and heat transfer coefficient versus mass flow rate: (a) 600 mm length, (b) 1000 mm length, (c) 800 mm length, and (d) maximum heat transfer coefficient and minimum pressure drop among all configurations.

Also, the pressure loss in the shell side nozzles (ΔP_{ns}) was considered through equation (21), where G_{ns} is a shell side nozzle mass velocity and n_s is the number of tube passes.

$$\Delta P_{ns} = 2.0 \times 10^{-13} \frac{n_s G_{ns}^2}{s_s}. \quad (21)$$

Then, the net pressure drop (ΔP_s) across the cold fluid stream on the shell side should be computed by summing the nozzle pressure loss and initial shell side pressure losses as per

$$\Delta P_s = \Delta P_o + \Delta P_{ns}. \quad (22)$$

5. Results and Discussion

5.1. Effect on the Pressure Drop and the Heat Transfer Coefficient. Figures 4(a)–4(c) show the pressure drop together with heat transfer coefficient variations within the STHX with the length of 600 mm, 800 mm, and 1000 mm for three different tube outer diameters of 10 mm, 12 mm, and 14 mm with 1 mm thick for each, respectively, through a given range of mass flow of 0.1-0.8 kg/s as regards the shell side. From Figures 4(a)–4(c), it can be seen that both the heat transfer coefficient and the pressure drop increase proportionally to the mass flow rate by considering the nine configurations of heat exchangers. Also, confirm that the heat transfer coefficient is much greater at any point in the range of mass flow rate compared to the pressure drop. Hence, it is noted that the diameter of 10 mm shows the greatest heat

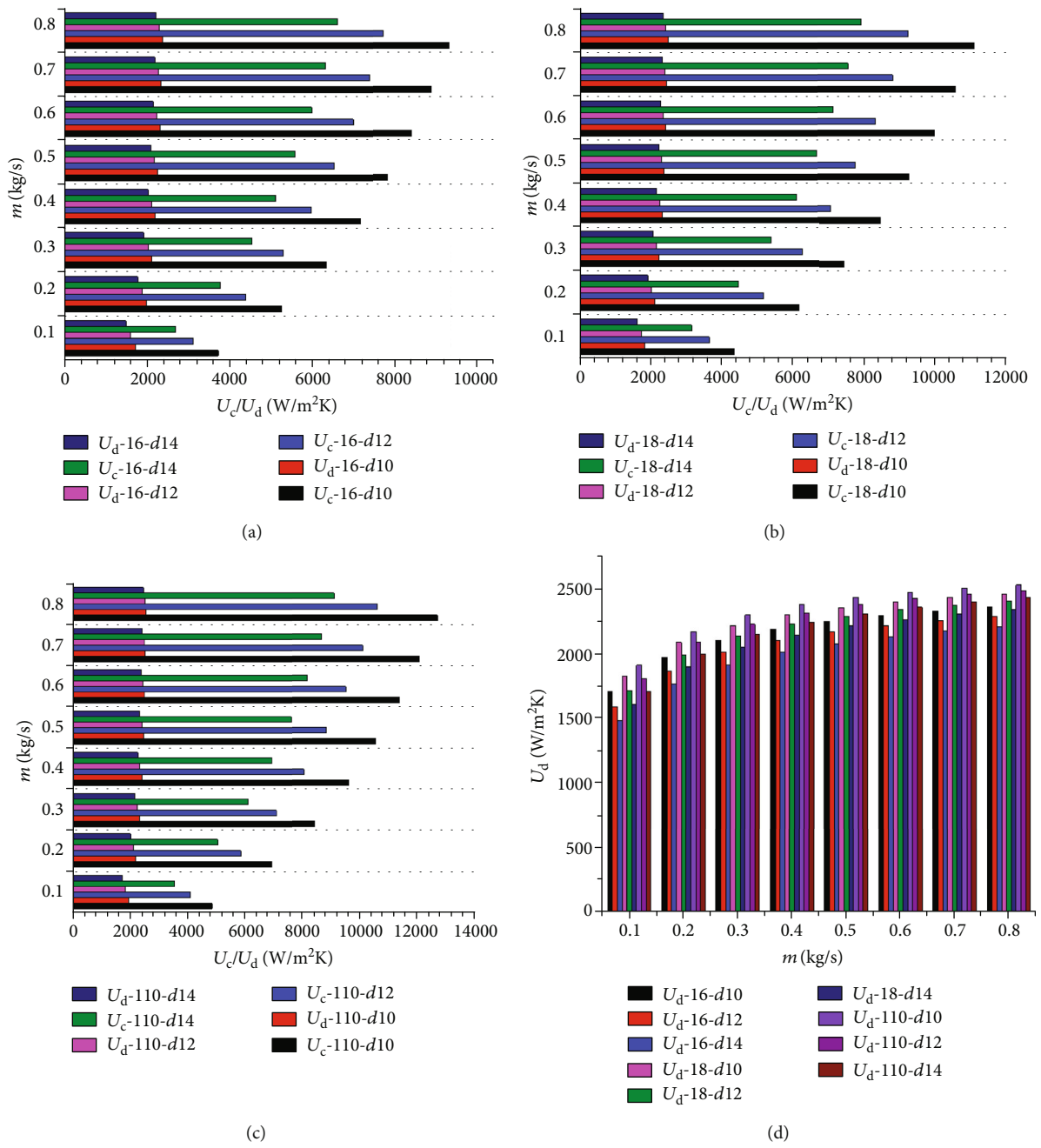

Figure 5: Overall heat transfer coefficient versus mass flow rate: (a) 600 mm length, (b) 800 mm length, (c) 1000 mm length, and (d) design overall heat transfer coefficient among all configurations.

transfer coefficient of 18162, 20881, and 23212 W/m^{2}K and the maximum pressure drop of 0.328, 0.593, and 0.957 Pa, while the diameter of 14 mm shows a minimum pressure drop of 0.117, 0.223, and 0.370 Pa and a lesser heat transfer coefficient of 13265, 15326, and 17107 W/m^{2}K in the length of 600 mm, 800 mm, and 1000 mm, respectively.

Figure 4(d) illustrates the variation of all minimum pressure drop (blue) which appears in the tube with a diameter of 14 mm versus the cold fluid stream mass flow rate in the shell side for the three different tube length exchangers. The results show that the tube configuration with a minimum length (600 mm) has a minimum pressure drop of 0.117 Pa corresponding to the rest of the configurations. Figure 4(d) also shows the results of the variation of the maximum heat transfer coefficient (black) which appears in the tube with a diameter of 10 mm versus cold stream mass flow rate in the shell side for the three different tube length exchangers; thus, the tube configuration with a maximum length of 1000 mm portrays maximum heat transfer coefficient of 23212 W/m^{2}K compared to the rest of the configurations.

5.2. Effect on the Overall Heat Transfer Coefficient. Figures 5(a)–5(c)) express the effect of mass flow rate on the overall heat transfer coefficients of design heat transfer

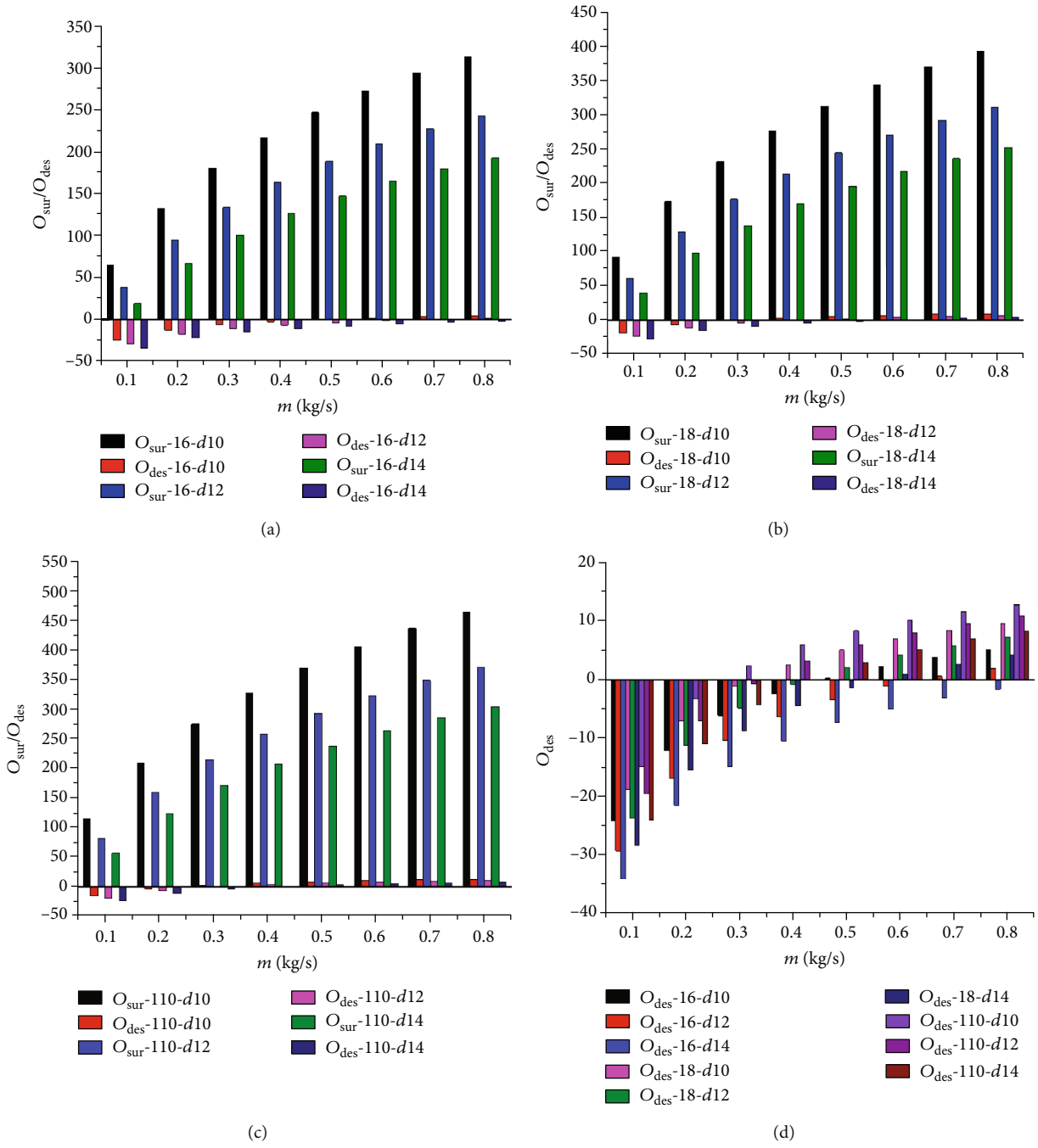

FIGURE 6: Oversurface and overdesign versus mass flow rate: (a) 600 mm length, (b) 800 mm length, (c) 1000 mm length, and (d) overdesign among all configurations.

coefficient (U_d) and clean heat transfer coefficient (U_c) within the STHX with the length of 600 mm, 800 mm, and 1000 mm for three different tube outer diameters of 10 mm, 12 mm, and 14 mm, respectively, with 1 mm thick for each. The results for both U_d and U_c coefficients demonstrate that when the cold fluid flows over the whole surface of the shell were varied, U_d and U_c increase constantly at any rate regardless of the difference in the tube configuration throughout the study. On the other hand, U_c is shown to increase twice or more than U_d when there is an increase in mass flow in the shell side. This is due to the significant effect of the fouling factor of the working fluids. However, the increase in mass flow and sustaining the temperatures keep U_d and U_c rising proportionally; the design coefficient is used rather than the clean coefficient based on the interest of overdesign. The highest and smallest values of U_d appeared in 10 and 14 mm tube diameter, respectively.

Figure 5(d) illustrates U_d which appears through all-tube configurations. The result shows that the tube configuration with a maximum length (1000 mm) has maximum U_d compared to the other configurations. Moreover, it can be seen that as the length of the tube increases with a decrease in

diameter the maximum U_d is achieved. To provide the required rate of heat transfer, the value of U_d should be greater than or equal to the value of the required coefficient, U_{req}. The results show that the suitable mass flow of 0.3-0.8 kg/s with a range of 2306-2539 W/m^{2}K can be selected for the proper design of the exchanger as shown in Figure 6(d).

5.3. Effect on the Oversurface and Overdesign. Figures 6(a)–6(c) demonstrate the oversurface (O_{sur}) and overdesign (O_{des}) changes when designing the STHX with the length of 600 mm, 800 mm, and 1000 mm for three different tube outer diameters of 10 mm, 12 mm, and 14 mm with 1 mm thick for each, respectively, through a given range of 0.1-0.8 kg/s. Since U_{req} is much smaller than U_c, O_{sur} appeared to increase in the range of 19.2-463.3 as the mass flow increases. O_{des} were shown to increase slightly from negative value on 0.1-0.3 kg/s to a positive value on 0.4-0.8 kg/s in a range of -33.9-12.8.

Since engineers do recognize that there will be uncertainties on the data provided and that there may be times when the feedstock will not exactly match up to what was originally specified, a certain amount of conservatism will be required just to achieve satisfactory performance despite unforeseen circumstances. Figure 6(d) clarifies the possibility of designing the suitable STHX by displaying the greatest values of O_{des} which mostly appeared in the smallest tube diameter (10 mm) to all three tube length configurations with a total of nine samples. However, O_{des} is a negative value at a low mass flow rate of 0.1-0.3 kg/s specifically to the configurations of length 600 mm and 800 mm. Conversely, as mass flow increases from 0.4 to 0.8 kg/s, O_{des} becomes a positive value. Hereafter, the configuration with tube length 1000 mm performed well even from the mass flow of 0.3 kg/s compared to other configurations.

6. Conclusion

A heat exchanger model for a low-temperature desalination system was established through the influence tube length and diameter, mass flow rate on pressure drop, heat transfer coefficient, overall heat transfer coefficient, oversurface, and overdesign. After making a deep analysis of these heat transfer parameters, the following summarized conclusions were obtained.

(i) Both the heat transfer coefficient and the pressure drop increase proportionally to the mass flow rate among all nine configurations of heat exchangers. But the pressure drop is noticed to be very low 0.328-0.957 Pa for all studied configurations that will lower the pumping power

(ii) The clean overall heat transfer coefficient increases twice or more to that of the design coefficient when there is an increase in mass flow in the shell side due to the effect of the fouling factor

(iii) The maximum design coefficient is achieved by increasing the tube length with a decrease in diameter. Also, the mass flow of 0.3-0.8 kg/s is suitable for the proper design of exchanger in the present study

(iv) The configuration with the 1000 mm length and 10 mm diameter which provides high heat transfer is recommended to work with a maximum flow rate of 0.8 kg/s to achieve a maximum heat transfer coefficient of 23212 W/m^{2}K, while 12.8 is a maximum overdesign coefficient achieved on 0.8 kg/s mass flow

(v) Therefore, the implementation of the proposed layout will ensure less energy consumption in the system. Hence, an experimental study is recommended to be done to compare the results obtained by the present mathematical model

Nomenclature

A: Area (m^2)
Cp: Specific heat capacity (kJ/kg)
D, d: Diameter (m)
$\dot{m}$: Mass flow rate (kg/s)
n: Pass number, number
F_t: Correction factor
f_t: Darcy friction factor
G: Mass velocity (kg/s m^2)
h: Heat transfer coefficient (W/m^{2}K)
k: Thermal conductivity (W/m K)
Q: Heat load (kW)
t: Temperature (°C)
s: Specific gravity
U: Overall heat transfer coefficient (W/m^{2}K)
Pr: Prandtl number
Re: Reynolds number.

Greek Letters

μ: Viscosity (kg/m s)
ρ: Density (kg/m^3)
ΔP: Pressure drop (Pa)
ΔT: Temperature difference (K).

Subscripts

6: Hot fluid inlet
7: Hot fluid outlet
2: Cold fluid inlet
3: Cold fluid outlet
b: Baffle
c: Clearance, clean
d: Design
e: Equivalent
f: Liquid, cold fluid
t: Tube
g: Vapor, gas, steam
w: Water
i: Initial, inner
r: Return
req: Required
lm: Logarithmic mean

n: Nozzles
m: Material, mean
s: Shell
o: Outer.

Abbreviations

STHX: Shell-and-tube heat exchanger.

Data Availability

The data used to support the findings of this study are available from the corresponding author upon request.

Conflicts of Interest

There are no conflicts to declare.

Acknowledgments

The authors would like to acknowledge the Arusha Technical College for allowing performing this study.

References

[1] Q. Chen, M. Kum Ja, Y. Li, and K. J. Chua, "Evaluation of a solar-powered spray-assisted low-temperature desalination technology," *Applied Energy*, vol. 211, pp. 997–1008, 2018.

[2] M. Maria Antony Raj, K. Kalidasa Murugavel, T. Rajaseenivasan, and K. Srithar, "A review on flash evaporation desalination," *Desalination and Water Treatment*, vol. 57, no. 29, pp. 13462–13471, 2015.

[3] Q. Chen, M. K. Ja, Y. Li, and K. J. Chua, "Energy, economic and environmental (3E) analysis and multi-objective optimization of a spray-assisted low-temperature desalination system," *Energy*, vol. 151, pp. 387–401, 2018.

[4] V. G. Gude and N. Nirmalakhandan, "Desalination at low temperatures and low pressures," *Desalination*, vol. 244, no. 1-3, pp. 239–247, 2009.

[5] S. Al-Kharabsheh and D. Yogi, "Analysis of an innovative water desalination system using low-grade solar heat," *Desalination*, vol. 156, no. 1-3, pp. 323–332, 2003.

[6] R. Roy, "Optimization of design parameters on shell and tube heat exchangers using flower pollination algorithm based on economic dispatch," *International Journal for Emerging Research and Development*, vol. 1, no. 5, pp. 11–15, 2018.

[7] S. M. Alsadaie and I. M. Mujtaba, "Dynamic modelling of heat exchanger fouling in multistage flash (MSF) desalination," *Desalination*, vol. 409, pp. 47–65, 2017.

[8] B. Ghorbani, R. Shirmohammadi, M. Amidpour, F. Inzoli, and M. Rocco, "Design and thermoeconomic analysis of a multi-effect desalination unit equipped with a cryogenic refrigeration system," *Energy Conversion and Management*, vol. 202, p. 112208, 2019.

[9] E. Elsayed, R. al-Dadah, S. Mahmoud, P. Anderson, and A. Elsayed, "Experimental testing of aluminium fumarate MOF for adsorption desalination," *Desalination*, vol. 475, p. 114170, 2020.

[10] C. Olkis, S. Brandani, and G. Santori, "Cycle and performance analysis of a small-scale adsorption heat transformer for desalination and cooling applications," *Chemical Engineering Journal*, vol. 378, p. 122104, 2019.

[11] K. Thu, Y. D. Kim, A. Myat, A. Chakraborty, and K. C. Ng, "Performance investigation of advanced adsorption desalination cycle with condenser–evaporator heat recovery scheme," *Desalination and Water Treatment*, vol. 51, no. 1-3, pp. 150–163, 2012.

[12] H. Rezk, A. S. Alsaman, M. al-Dhaifallah, A. A. Askalany, M. A. Abdelkareem, and A. M. Nassef, "Identifying optimal operating conditions of solar-driven silica gel based adsorption desalination cooling system via modern optimization," *Solar Energy*, vol. 181, pp. 475–489, 2019.

[13] S.-Y. Woo, H. S. Lee, H. Ji, D. S. Moon, and Y. D. Kim, "Silica gel-based adsorption cooling cum desalination system: focus on brine salinity, operating pressure, and its effect on performance," *Desalination*, vol. 467, pp. 136–146, 2019.

[14] A. David, R. K. Sinha, and J. M. Paul, "Feasibility of working of evaporative condenser cum thermal desalination system," *International Journal of Innovative Research in Technology*, vol. 5, no. 8, pp. 79–82, 2019.

[15] K. Rabhi, R. Nciri, F. Nasri, C. Ali, and H. Ben Bacha, "Experimental performance analysis of a modified single-basin single-slope solar still with pin fins absorber and condenser," *Desalination*, vol. 416, pp. 86–93, 2017.

[16] B. Chandrakanth, G. Venkatesan, L. S. S. Prakash Kumar, P. Jalihal, and S. Iniyan, "Thermal design, rating and second law analysis of shell and tube condensers based on Taguchi optimization for waste heat recovery based thermal desalination plants," *Heat and Mass Transfer*, vol. 54, no. 9, pp. 2885–2897, 2018.

[17] Y. Matsuda, Y. Eishima, S. Goto et al., "Construction of water level model for after condenser in spray flash desalination system via stochastic process," in *Proceedings of the 49th ISCIE International Symposium on Stochastic System Theory and Its Applications*, Hiroshima, Japan, 2017.

[18] H. Xu, X. Sun, and Y. Dai, "Thermodynamic study on an enhanced humidification-dehumidification solar desalination system with weakly compressed air and internal heat recovery," *Energy Conversion and Management*, vol. 181, pp. 68–79, 2019.

[19] S. Kakaç, H. Liu, and A. Pramuanjaroenkij, *Heat exchangers: selection, rating, and thermal design*, CRC press, 2002.

[20] B. Sundén and R. M. Manglik, *Plate heat exchangers: design, applications and performance*, vol. 11, Wit Press, 2007.

[21] A. A. A. Arani and R. Moradi, "Shell and tube heat exchanger optimization using new baffle and tube configuration," *Applied Thermal Engineering*, vol. 157, p. 113736, 2019.

[22] M. Nitsche and R. O. Gbadamosi, *Heat exchanger design guide: a practical guide for planning, selecting and designing of shell and tube exchangers*, Butterworth-Heinemann, 2015.

[23] R. Lord, P. Minton, and R. Slusser, "Design of heat exchangers," *Chemical Engineer*, vol. 77, no. 2, pp. 96–118, 1970.

[24] A. S. Ambekar, R. Sivakumar, N. Anantharaman, and M. Vivekenandan, "CFD simulation study of shell and tube heat exchangers with different baffle segment configurations," *Applied Thermal Engineering*, vol. 108, pp. 999–1007, 2016.

[25] C. Gonçalves, A. L. H. Costa, and M. J. Bagajewicz, "Linear method for the design of shell and tube heat exchangers using the Bell–Delaware method," *AICHE Journal*, vol. 65, no. 8, p. 8, 2019.

[26] D. Y. Goswami, *The CRC Handbook of Mechanical Engineering*, CRC press, 2004.

[27] G. Towler and R. Sinnott, *Chemical engineering design: principles, practice and economics of plant and process design*, Elsevier, 2012.

[28] R. W. Serth and T. Lestina, *Process heat transfer: principles, applications and rules of thumb*, Academic press, 2014.

[29] K. Thulukkanam, *Heat Exchanger Design Handbook*, CRC press, 2013.

[30] N. M. Khalfe, K. S. Lahiri, and K. S. Wadhwa, "Simulated annealing technique to design minimum cost exchanger," *Chemical Industry and Chemical Engineering Quarterly/CI-CEQ*, vol. 17, no. 4, pp. 409–427, 2011.